Biophysical Journal Volume 106 May 2014 2184–2195

Characterization of the Connexin45 Carboxyl-Terminal Domain Structure and Interactions with Molecular Partners

Jennifer L. Kopanic, Mona H. Al-mugotir, Fabien Kieken, Sydney Zach, Andrew J. Trease, and Paul L. Sorgen*
Department of Biochemistry and Molecular Biology, University of Nebraska Medical Center, Omaha, Nebraska

ABSTRACT Mechanisms underlying the initiation and persistence of lethal cardiac rhythms are of significant clinical and scientific interests. Gap junctions are principally involved in forming the electrical connections between myocytes, and changes in distribution, density, and properties are consistent characteristics in arrhythmic heart disease. Therefore, understanding the structure and function of gap junctions during normal and abnormal impulse propagation are essential in the control of arrhythmias. For example, Cx45 is predominately expressed in the specialized myocytes of the impulse generation and conduction system. In both ventricular and atrial human working myocytes, Cx45 is present in very low quantities. However, a reduction in Cx43 coupled with an increased Cx45 protein levels within the ventricles have been observed after myocardial infarction and end-stage heart failure. Cx45 may influence electrical and/or metabolic coupling as a result of pathophysiological overexpression. Our goal was to identify mechanisms that could cause cellular coupling to be different between the cardiac connexins. Based upon the conserved transmembrane and extracellular loop segments, our focus was on identifying features within the divergent cytoplasmic portions. Here, we biophysically characterize the carboxyl-terminal domain of Cx45 (Cx45CT). Purification revealed the possibility of oligomeric species, which was confirmed by analytical ultracentrifugation experiments. Sedimentation equilibrium and circular dichroism studies of different Cx45CT constructs identified one region of α-helical structure (A333-N361) that mediates CT dimerization through hydrophobic contacts. Interestingly, the binding affinity of Cx45CT dimerization is 1000-fold stronger than Cx43CT dimerization. Cx45CT resonance assignments were also used to identify the binding sites and affinities of molecular partners involved in the Cx45 regulation; although none disrupted dimerization, many of these proteins interacted within one intrinsically disordered region (P278-P285). This domain has similarities with other cardiac connexins, and we propose they constitute a master regulatory domain, which contains overlapping molecular partner binding, *cis-trans* proline isomerization, and phosphorylation sites.

INTRODUCTION

Gap junctions are conglomerates of cell-to-cell channels that allow for the direct exchange of ions and low molecular mass metabolites (<1 kDa) between adherent cells. They provide a pathway for the propagation and/or amplification of signal transduction cascades triggered by cytokines, growth factors, and other cell signaling molecules involved in growth and development. Gap junction channels are created by the apposition of connexons from adjacent cells, in which each connexon is formed by six connexin proteins. There are 21 different human connexin isoforms named according to their molecular mass (e.g., 45 kDa isoform is Cx45) with differential spatial-temporal tissue expression (1). For example, Cx45, Cx43, and Cx40 are found in distinct combinations and relative quantities in different, functionally specialized subsets of cardiomyocytes (2). In the diseased heart, expression levels of these cardiac connexins are altered, which can lead to abnormal impulse propagation and generation of ventricular arrhythmias, predisposing patients to heart failure (3–5). Even though there is a significant amount of sequence homology between the connexins, the major divergence in primary structures, which helps confer specific regulatory properties for each isoform, occurs in the cytoplasmic loop and carboxyl terminal (CT) domains.

The CT domain plays a role in the trafficking, size, localization, and turnover of gap junctions, as well as the level of intercellular coupling via numerous posttranslational modifications and protein-protein interactions (6–8). Structural studies of Cx43 and Cx26 gap junctional channels, which used cryo-electron microscopy and x-ray crystallography techniques, respectively, provided a significant amount of information about channel architecture (9,10). Unfortunately, neither technique was able to determine the CT structure because of its dynamic nature. More amendable biophysical techniques, such as NMR and circular dichroism (CD), have been used to study the CT domain. NMR was used to assign the resonances of the soluble Cx43CT (S255-I382) and Cx40CT (S251-V355) domains and determined they are predominantly intrinsically disordered in structure (11–14). This information was used to map the binding sites, calculate the binding affinities of molecular partners, and determine the effects of pH and phosphorylation on these interactions (13–17). Together with biophysical studies of the Cx43CT and Cx40CT domains from other laboratories, mechanisms involved in channel gating and protein turnover have been identified (18–26). To date, little information exists for the CT domain from the Cx45 isoform (Cx45CT; (27,28)). Therefore, we

Submitted October 1, 2013, and accepted for publication March 31, 2014.
*Correspondence: psorgen@unmc.edu
Editor: David Eliezer.

0006-3495/14/05/2184/12 $2.00
http://dx.doi.org/10.1016/j.bpj.2014.03.045

characterized the biophysical properties of the Cx45CT domain and its interactions with molecular partners involved in gap junction regulation. The information provided herein offers a better understanding of the similarities and differences in structure and binding of protein partners between the cardiac connexin CT domains that can be exploited to aid in the design of chemical modifiers to regulate the function of gap junctions.

MATERIAL AND METHODS

Cloning, expression, and purification of the Cx45CT domain, truncation A333-N361, Cx45 4th transmembrane (TM4) domain, and Cx45CT attached to the TM4 domain

DNA encoding the Cx45CT (K265-I396) and the Cx45CT attached to the 4th transmembrane domain (TM4-Cx45CT; D219-I396) were cloned using polymerase chain reaction from a BlueScribe SK vector containing the *Mus musculus Cx45* gene (gift from Dr. Steven M. Taffet) into the bacterial expression vector pGEX-KT (gift from Dr. Gregory S. Taylor) and pET-14b (Novagen; Madison, WI), respectively. The plasmid sequences (and others described below) were verified at the University of Nebraska Medical Center DNA Sequencing Core Facility. The domain boundary for the Cx45CT begins at K265, placing this residue close but outside of the TM4 (transmembrane prediction programs: http://www.cbs.dtu.dk/services/TMHMM/ and http://www.ch.embnet.org/software/TMPRED_form.html). The protocols used to express and purify the Cx45CT and TM4-Cx45CT domains were previously described (27,28). The TM4 domain was purified using the same procedures as the TM4-Cx45CT. Unless noted, the final buffer condition used in all experiments was 1× phosphate buffered saline (PBS) buffer at pH 5.8 and 25°C for the Cx45CT domain and 20 mM MES, 50 mM NaCl, 8% w/v 1-palmitoyl-2-hydroxy-*sn*-glycero-3-[phospho-RAC-(1-glycerol)] (LPPG; Avanti Lipids; Alabaster, AL), 1 mM DTT, and 1 mM EDTA at pH 5.8 and 42°C for the TM4 and TM4-Cx45CT domains.

Cx45CT residues A333-N361 were cloned using polymerase chain reaction from the Cx45CT K265-I396 construct into the pGEX-KT vector. The boundaries were chosen based on the Cx45CT residues that broadened beyond detection in the ^{15}N-HSQC experiment (27). The polypeptide was transformed with Rosetta 2(DE3)pLysS cells (Novagen), grown in either Luria Broth (LB) or ^{15}N-labeled minimal media, and induced with 0.5 mM IPTG (final concentration) at a cell density of 0.6 OD_{600} for 4 h. The bacterial cells were pelleted and resuspended in 1× PBS, 1 mM PMSF, 1% v/v NP-40, and Complete Protease Inhibitor (Roche Molecular Biochemicals; Mannheim, Germany). The cells were lysed using a French Press and the lysate was cleared by centrifugation (16,500 rpm, 1 h). The GST-tagged Cx45CT A333-N361 domain was incubated with GST resin (GenScript; Piscataway, NJ) for 2 h at 4°C and cleaved from the GST-tag by incubation with thrombin overnight. The Cx45CT A333-N361 was then incubated with benzamidine resin (GE Healthcare; Pittsburgh, PA) and concentrated using Amicon Ultra 3 K and 30 K filters (Millipore; San Diego, CA). The final buffer condition used (unless noted) was 1× PBS buffer at pH 5.8 and 25°C.

Expression and purification of other GST-tagged proteins

Protein domains cloned in the pGEX-KT vector include neural precursor cell expressed developmentally downregulated protein 4 (Nedd4) WW2 (D392-S458) domain (gift from Dr. Daniela Rotin) and c-Src Src Homology 3 (SH3, G81-V147) domain (14,15). Protein domains cloned into the pGEX-6P-2 vector include Dynamin 2 (Dyn2; gift from Dr. Steve Caplan) pleckstrin homology (PH; V520-K629) domain, Cx43CT (V236-I382), and Cx40CT (S251-V355) (12,14,17,29). These proteins were expressed using BL21(DE3) competent cells (Life Technologies) and purified using techniques described previously for the Cx45CT A333-N361 construct. To cleave the protein of interest from GST, beads were incubated overnight at 4°C with thrombin (pGEX-KT vector) or Turbo3C (Accelagen; San Diego, CA; pGEX-6P-2 vector).

Cloning, expression, and purification of His-tagged proteins

The ZO-1 PDZ-2 (T185-E264) domain was cloned into the pET-14b vector (14,15,30). DNA containing the tumor susceptibility gene 101 (TSG101) Ubiquitin E2 Variant (UEV, M1-P145) domain in the pET-28a vector was a gift from Dr. Kay-Uwe Wagner. After expression using BL21(DE3) cells as described previously for GST-tagged proteins, the bacterial cell pellet was resuspended in 1× PBS, 20 mM imidazole, and 1 mM β-mercaptoethanol at pH 5.8 with protease inhibitor cocktail (Sigma Aldrich; St. Louis, MO), then lysed three times using the French Press. The lysate was cleared by centrifugation (17,500 rpm, 1 h, 4°C). The supernatant was loaded onto an ÄKTA FPLC using a HisTrap HP column (GE Healthcare). Protein elution was accomplished using a gradient (0–100%) of 1× PBS, 1 M imidazole, and 1 mM β-mercaptoethanol at pH 5.8. Fractions containing purified protein were verified by SDS-PAGE, pooled, and dialyzed overnight at 4°C against 1× PBS with 1 mM DTT at pH 5.8 using a 3 kDa cut-off Slide-A-Lyzer dialysis cassette (Pierce; Rockford, IL).

Expression and purification of calmodulin

DNA encoding calmodulin (CaM) in the pAED7 vector was a gift from Dr. Katalin Török. The protocol used to express and purify CaM was previously described (31,32). After purification, CaM was lyophilized and stored at −20°C. Desired amounts were weighed and solubilized in a solution of 100 mM KCl and 10 mM $CaCl_2$ at pH 6.0.

Circular dichroism (CD) spectroscopy

CD experiments were performed using a Jasco J-815 spectrophotometer fitted with a Peltier temperature control system (Easton, MD). The CD spectra for the Cx45CT K265-I396 and A333-N361 domains were recorded in various buffer conditions (Table S1 in the Supporting Material). For each sample, 5 scans (wavelength range: 300–190 nm; response time: 1 s; scan rate: 50 nm/min; bandwidth 1.0 nm) were collected using a 0.01 cm quartz cell and processed using Spectra Analysis (Jasco). Each spectrum shown is the mean residue ellipiticity (MRE; deg cm^2 dmol^{-1}) as a function of wavelength and average of 5 scans. All spectra are corrected by subtracting the solvent spectrum. Protein concentrations were determined using a NanoDrop 1000 (Thermo Scientific; Wilmington, DE) or Biospec 1601 UV-VIS spectrophotometer (Shimadzu; Carlsbad, CA) at 280 nm. Analyses of spectra were performed using the Provencher and Glockner method with the SP175 reference set on the online program DichroWeb (33–36).

Analytical ultracentrifugation – sedimentation equilibrium

Sedimentation equilibrium experiments were performed at 20°C with a Beckman Optima XL-I analytical ultracentrifuge using an AN-50Ti or AN-60Ti rotor (Beckman Coulter; Indianapolis, IN). For sedimentation equilibrium, different Cx45CT constructs were analyzed in various buffer conditions (Table S1). Data were collected at three concentrations (Abs_{280nm} of 0.3, 0.5, and 0.9) and various rotor speeds. Absorbance scans

at 280 nm were taken after 18 h, 20 h, and 24 h at each speed; equilibrium was reached if the scans were unchanged. Analysis of the sedimentation equilibrium data was performed using the Beckman XL-A/XL-I software package within Microcal, ORIGIN v4. The software Sednterp (http://www.rasmb.bbri.org) was used to calculate the buffer viscosities and densities as well as the partial specific volume for each protein based on the amino acid composition.

Nuclear magnetic resonance

All NMR data were acquired using a 600 MHz Varian INOVA NMR Spectrometer outfitted with a cryo-probe at the University of Nebraska Medical Center's NMR Facility. NMR spectra were processed and phased using NMRPipe and NMRDraw (37,38) and analyzed using NMRView (37). Gradient-enhanced two-dimensional ^{15}N-HSQC experiments were acquired with 1024 complex points in the direct dimension and 256 complex points in the indirect dimension (39). Sweep widths were 10,000 Hz in the ^{1}H dimension and 2,430.6 Hz in the ^{15}N dimension. Diffusion ordered spectroscopy data were collected using a 400 MHz Bruker spectrometer and processed using TopSpin (Bruker).

RESULTS

Dimerization of the Cx45CT domain

Two independent observations suggested the ability of the Cx45CT domain to oligomerize. First, the 15 kDa Cx45CT was unable to pass through a 30 kDa molecular cut off filter, unlike the similar molecular mass Cx43CT and Cx40CT domains (13,29). Second, a yeast two-hybrid screen using the Cx45CT domain as bait against a cardiac cDNA library identified an interaction against itself (data not shown). Therefore, sedimentation equilibrium experiments were performed to confirm Cx45CT oligomerization, determine the oligomerization state, and calculate the dissociation constant (K_D). Data were collected at either physiological (pH 7.5) or acidic (pH 5.8) conditions. Intracellular acidification, which is a major consequence of tissue ischemia during a myocardial infarction, leads to closure, degradation, and altered expression of gap junction channels and can be a substrate for malignant ventricular arrhythmias (2). Plots of optical density at equilibrium as a function of radius at pH 5.8 and 7.5 at a rotor speed of 22,000 rpm are shown in Fig. 1, *A* and *B*, respectively. Data were also collected at 18,000 and 26,000 for both pH values (Fig. S1) and used to analyze the stoichiometry of oligomerization. Each plot was best fit by a function derived from a self-association model that determined the fraction of protein in specific oligomeric states (Beckman XL-A/XL-I software package). The molecular mass values were determined to be 31,152 Da at pH 5.8 and 31,435 Da at pH 7.5. A dimer model showed very good convergence as demonstrated by the minimum deviation in the residuals (top plot on each panel) and a weighted variance approaching unity (data not shown). In contrast, fits of data to a monomer, monomer-dimer-trimer, and monomer-dimer-tetramer model had weighted variance values significantly greater than one. The results obtained from the dimer model

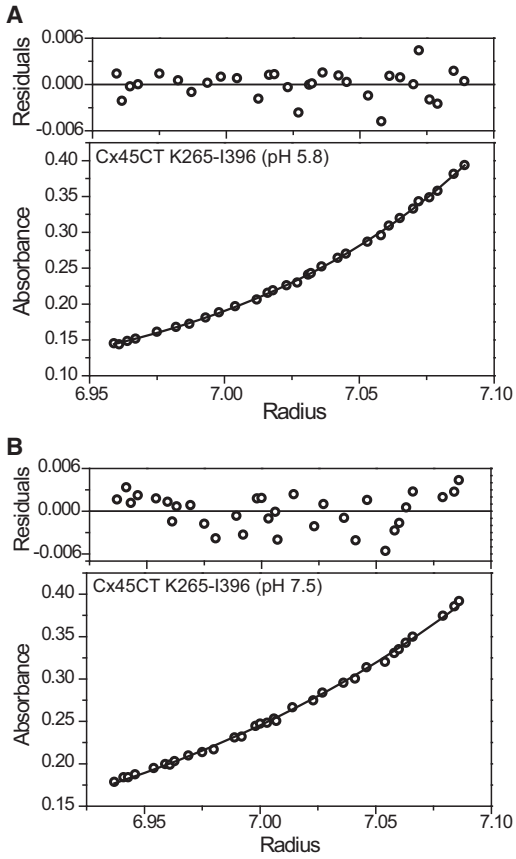

FIGURE 1 Distribution of the Cx45CT domain at sedimentation equilibrium. Absorbance of the Cx45CT domain in 1× PBS buffer at (*A*) pH 5.8 and (*B*) pH 7.5 at equilibrium (22,000 rpm) are shown as a function of radius. The solid lines are the theoretical curves.

were used to calculate the K_D (141 nM at pH 5.8 and 97 nM at pH 7.5). Sedimentation velocity was then used to provide an independent confirmation of the oligomeric state (Fig. S2). Two species were discerned for the Cx45CT at both pH 5.8 and pH 7.5 corresponding to the sedimentation coefficient distribution *c(s)* at s_{20w}-values of 2.165 S (major) and 0.2545 S (minor) at pH 5.8 and 2.045 S (major) and 0.2374 S (minor) at pH 7.5. The molecular mass values of the major species implied by the average boundary spread in the sedimentation coefficient distribution $c(s)$ were 32,630 Da at pH 5.8 and 32,604 Da at pH 7.5.

Secondary structure of the Cx45CT domain

CD spectroscopy was used to determine which type of secondary structure mediates Cx45CT dimerization. The CD spectra of the Cx45CT domain at both pH 5.8 and 7.5 have two peak minima at 206 and 222 nm; however, the MRE value at 206 nm is more negative than the 222 nm MRE value (Fig. 2 *A*). The data are characteristic of a protein that contains both α-helical and random coil structures, which was confirmed by Dichroweb analysis (34–36). The Cx45CT domain at pH 5.8 and 7.5 were

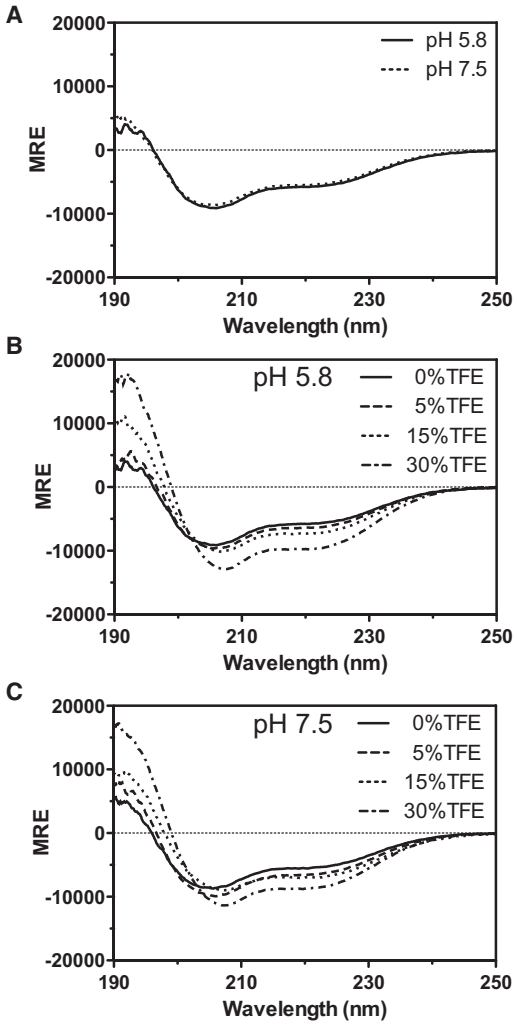

FIGURE 2 Secondary structure of the Cx45CT domain. (*A*) CD spectra of the Cx45CT domain at pH 5.8 and 7.5. CD spectra at (*B*) pH 5.8 and (*C*) pH 7.5 were also obtained in the presence of varying concentrations of 2,2,2-trifluoroethanol (TFE; % indicated in each panel).

19% and 18% α-helical, respectively, with the remainder of the protein being random coiled. CD measurements were also carried out in various concentrations of the helix-stabilizing cosolvent 2,2,2-Trifluoroethanol (TFE; Fig. 2, *B* and *C*). Increasing the TFE concentrations from 5% to 30% at both pH 5.8 and 7.5 caused a shift in the minima peaks from 206 nm to 208 nm, a decrease in the 222 nm values, and an increase in the 195 nm values, which indicate additional α-helical content. This result suggests that TFE is stabilizing the innate α-helical structure and/or residues susceptible to α-helical formation.

Characterizing Cx45CT residues A333-N361

The first indication of the residues involved in both dimerization and α-helical structure was derived from the ^{15}N-HSQC spectrum of the Cx45CT domain (27). Upon assignment of the resonances, one region (A333-N361) had crosspeaks that broadened beyond detection (Fig. 3 *A*), suggesting intermediate chemical exchange. Additionally, the small dispersion of the remaining crosspeaks in the ^{15}N-HSQC spectrum ($\leq$1 ppm) indicated a lack of secondary structure. Combined, these observations suggest that the Cx45CT residues A333-N361 contain the α-helical and may be responsible for the dimeric structure. These findings were confirmed by characterizing a polypeptide corresponding to Cx45CT residues A333-N361. The CD data indicate that Cx45CT residues A333-N361 are predominantly α-helical (Fig. 3 *B*). Sedimentation equilibrium data revealed that the Cx45CT A333-N361 polypeptide at pH 5.8 was also dimeric with a significantly increased binding affinity compared to the full-length Cx45CT (K_D = 74 pM, Fig. 3 *C* and Fig. S3).

Disruption of the dimerization domain

To ascertain the noncovalent forces responsible for dimerization within Cx45CT residues A333-N361, a helical wheel analysis was performed (Fig. 3 *D*). The data identified a hydrophobic (L335, I338, I342, A345, and L349) and an electrostatic (E336, R340, R343, E347, and D350) face. Therefore, different buffer conditions were screened to determine the face mediating Cx45CT dimerization (Table S1). The goal was to compare conditions that disrupt dimerization yet maintain the α-helical structure; highlighted in bold are solution conditions that met this goal. A commonality among them is their ability to disrupt hydrophobic interactions (40–42). Provided in Fig. 4 are the CD and sedimentation equilibrium data of representative solution conditions that disrupt either the electrostatic or hydrophobic interactions. The Cx45CT domain remains α-helical in both types of solution conditions but is monomeric in 30% acetonitrile (15,407 Da) and dimeric in 1 M NaCl (31,782 Da, K_D = 242 pM). Using sedimentation velocity, the sedimentation coefficient distribution $c(s)$ at s_{20w}-values for the Cx45CT in 30% acetonitrile was 1.155 S (Fig. S4). The molecular mass implied by the average boundary spread in the single sedimentation coefficient distribution $c(s)$ was 15,635 Da, showing that acetonitrile disrupted Cx45CT dimerization. Interestingly, increasing the concentration of NaCl to 1 M (from 137 mM in 1$\times$ PBS) caused an increase in the binding affinity of the Cx45CT dimer (242 pM vs. 141 nM); this salting out effect is consistent with dimerization being driven by the hydrophobic interactions. Similar findings were observed with the Cx45CT A333-N361 polypeptide.

In the presence of 30% acetonitrile, the Cx45CT A333-N361 polypeptide also remained α-helical and monomeric (3,631 Da; Fig. 5, *A* and *B*, and Fig. S5). Disruption of dimerization was evident upon comparison of the ^{15}N-HSQC spectra collected for the polypeptide in 1$\times$ PBS alone and with 30% acetonitrile at pH 5.8 (Fig. 5 *C*). The

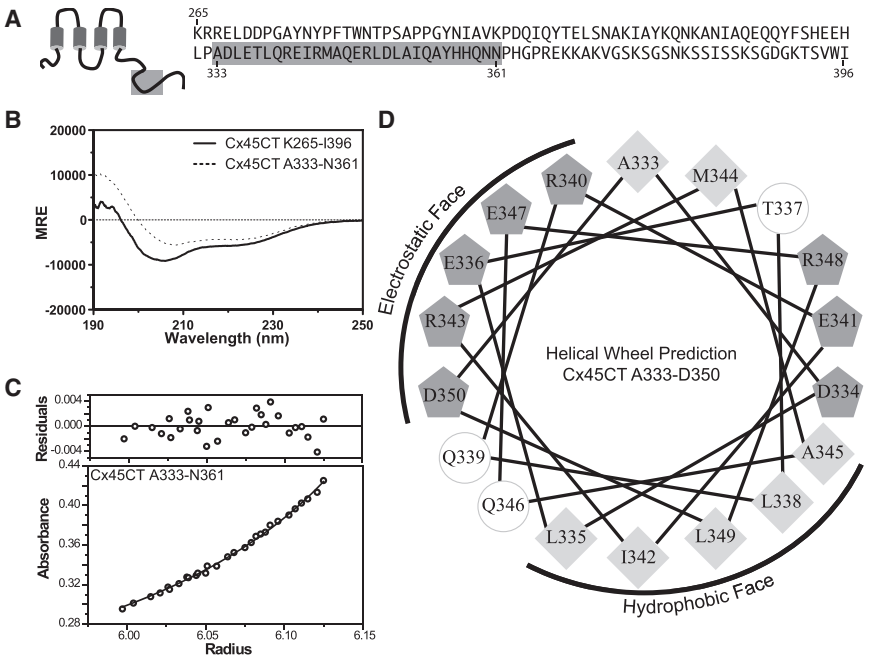

FIGURE 3 Characterization of the Cx45CT α-helical and dimerization domain. (*A*) Schematic diagram and primary amino acid sequence of the Cx45CT domain. Highlighted in gray are the residues not present in the ^{15}N-HSQC spectrum. (*B*), CD spectra of the Cx45CT domain: full-length (K265-I396) and polypeptide (A333-N361). (*C*) Sedimentation equilibrium of the Cx45CT polypeptide (A333-N361) is shown as a function of radius at 30,000 rpm. The solid line corresponds to the theoretical curve. (*D*) Helical wheel projection of Cx45CT residues A333-D350 showcases the hydrophobic and electrostatic faces. Hydrophilic residues are circles, hydrophobic residues are diamonds, and charged residues as pentagons.

1× PBS solution condition contains only 10 crosspeaks, whereas all 29 crosspeaks are visible in 30% acetonitrile. Together with the full-length Cx45CT, the A333-N361 polypeptide data strongly suggest dimerization is mediated by interactions involving the hydrophobic residues.

To determine the orientation of the dimer conformation, molecular modeling was performed using Cx45CT residues A333-N361. Initially, α-helical backbone hydrogen bonds were used as distance constraints of 1.60–2.05 Å between O_i and NH_{i+4} and 2.2–3.0 Å between O_i and N_{i+4} for residues in this segment. Structural models were then calculated from fully extended starting conformations using the protein structure calculation program CYANA (43). The 10 lowest energy structures were inputted into the protein docking program ZDOCK (44). ZDOCK searches all possible binding modes in the translational and rotational space between the two proteins and evaluates each by an energy scoring function. Of the 10 lowest energy structures, six were in a parallel and four in an antiparallel conformation. Next, all hydrogens within 5 Å between the two molecules

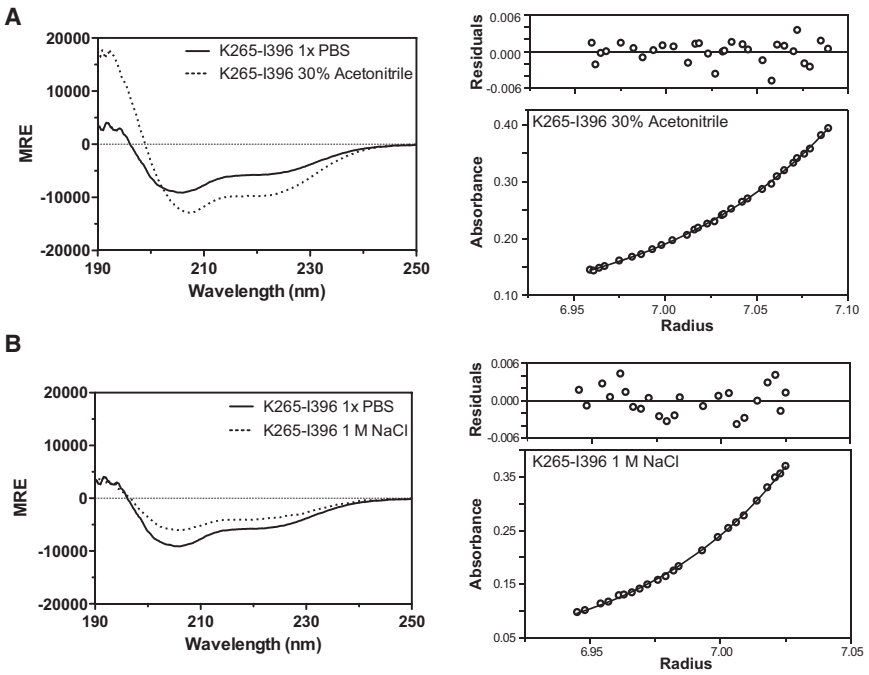

FIGURE 4 Identifying solution conditions that affect the Cx45CT dimer conformation without altering secondary structure. CD (*left*) and sedimentation equilibrium (*right*) data were collected for the Cx45CT domain in 1× PBS with (*A*) 30% acetonitrile or (*B*) 1 M NaCl at pH 5.8. For sedimentation equilibrium, the absorbances of the Cx45CT domain at equilibrium (18,000 rpm) are shown as a function of radius. The solid lines are the theoretical curves.

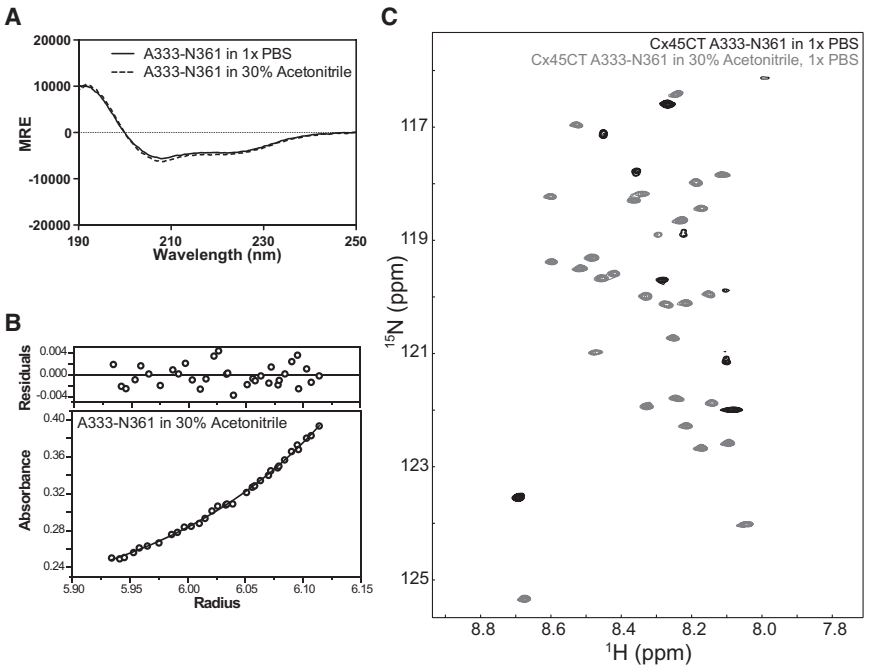

FIGURE 5 Acetonitrile disrupts dimerization of the Cx45CT polypeptide without altering secondary structure. CD (*A*) and sedimentation equilibrium (*B*) data (A) CD and (B) sedimentation equilibrium were collected for the Cx45CT polypeptide (A333-N361) in 1× PBS with 30% acetonitrile at pH 5.8. For sedimentation equilibrium, absorbance at equilibrium (30,000 rpm) is shown as a function of radius. The solid line is the theoretical curve. (*C*) ^{15}N-HSQC of the Cx45CT polypeptide (A333-N361) in 1× PBS (*black*) and 1× PBS with 30% acetonitrile (*gray*) at pH 5.8.

were identified for the lowest energy parallel and antiparallel conformations (Fig. 6, *A* and *B*). Based upon the number of residues involved (11 vs. 27) and total number of connectivities (61 vs. 193), the data support a parallel dimer conformation. Using the modeling software molmol, the lowest energy parallel dimer structure is illustrated in Fig. 6 *C*. Additionally, the online program COILS (predicts coiled-coil regions of proteins and peptides; http://embnet.vital-it.ch/software/COILS_form.html) predicted with a high probability (99%) that residues A333-N361 form a coiled-coil structure. This finding is consistent with the molecular modeling data as coiled-coil domains are involved in protein oligomerization.

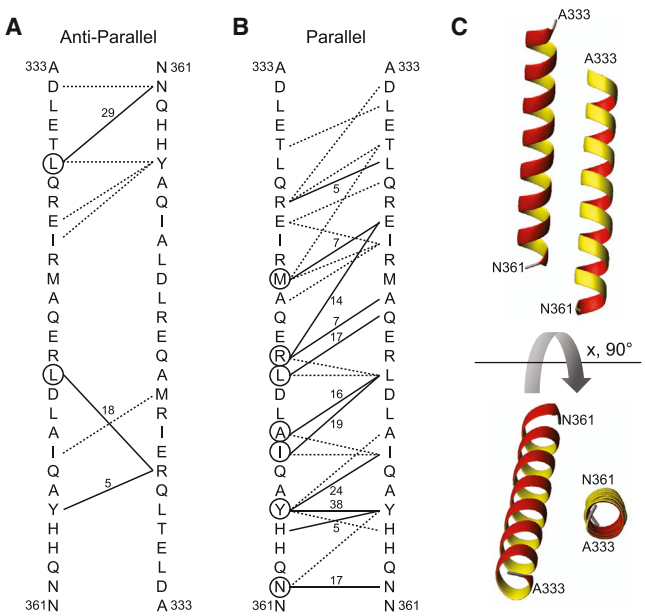

FIGURE 6 Intermolecular interactions responsible for Cx45CT dimerization. Displayed is Cx45CT residues A333-N361 in an (*A*) antiparallel and (*B*) parallel configuration. The lines between the Cx45CT domains represent the number of hydrogen bonds within 5 Å between the indicated residues. Solid lines have >5 connections (<5 have *dashed lines*). Circled residues contain >10 total connections. (*C*) Ribbon diagram of the lowest energy parallel conformation. To see this figure in color, go online.

To provide additional evidence that the hydrophobic face is mediating Cx45CT dimerization, all residues comprising the hydrophobic face where substituted (L335E, L338E, I342E, L349E, I353E, and Y356E). As a control, substitutions were made to residues along the electrostatic face (E336Q, R340Q, R343Q, E347Q, and D350Q). Both constructs maintain α-helical structure (Fig. S6). However, only substitutions of the hydrophobic residues inhibited dimerization (Fig. S7, Fig. S8, and Table S2). Altogether, these data further support that Cx45CT dimerization is based on hydrophobic interactions.

Characterizing the Cx45CT domain interaction with molecular partners

The identification of proteins that interact with each of the connexin CT domains has been instrumental toward a better understanding of gap junction regulation. Yet, as compared to other isoforms, little information is known about Cx45 molecular partners. Based upon the commonality of cardiac connexins to express within the same cell and to associate with ZO-1 (14,15,45–52), we tested if other known Cx43 and Cx40 molecular partners also interact with the Cx45CT domain (Table S3). ^{15}N-HSQC experiments were performed with each unlabeled molecular partner titrated at varying molar ratios into a buffer solution containing

^{15}N-Cx45CT at a constant concentration (100 μM). As controls, ^{15}N-HSQC spectra of the Cx45CT domain were collected in the presence of increased salt, bovine serum albumin, or calcium to identify resonances susceptible to nonspecific effects (Fig. 7 *A*). The changes in chemical shifts were plotted as a function of molecular partner concentration and fitted using the nonlinear least squares method to determine the K_D of the interactions. An example titration with the Nedd4 WW2 domain is provided in Fig. S9. In total, six molecular partners were studied, each with varying mechanisms to regulate gap junctions. A summary of the Cx45CT residues affected by each of the molecular partners with the K_D values is provided in Fig. 7 *B*. The ZO-1 PDZ-2 domain interacted with residues at the C-terminus of Cx45CT (K371-I396). The remaining molecular partners (c-Src SH3 domain, Nedd4 WW2 domain, TSG101 UEV domain, Dyn2 PH domain, and CaM) interacted near the N-terminus with varying binding affinities and between residues L269 and N314.

Cx45CT interaction with the Cx43CT and Cx40CT domains

The existence of heteromeric Cx40/Cx43, Cx45/43, Cx45/Cx40 connexons, the ability of Cx45CT, Cx43CT, and Cx40CT to dimerize, and the known interaction between the Cx43CT and Cx40CT domains suggest possible hetero-CT interactions involving the Cx45CT domain (4,13,14,27,29,50–52). To test for hetero-CT dimerization, ^{15}N-HSQC spectra were acquired using unlabeled Cx40CT or Cx43CT titrated at varying concentrations into a buffer solution containing ^{15}N-Cx45CT (100 μM). A summary of the Cx45CT residues affected by the presence of Cx43CT or Cx40CT are displayed in Fig. 7 *C*. The Cx40CT and Cx43CT domains affected residues in a similar area of the Cx45CT domain and with comparable K_D values.

In addition, ^{15}N-HSQC spectra were acquired using ^{15}N-labeled Cx43CT or Cx40CT (100 μM) with various molar ratios of unlabeled Cx45CT. The Cx45CT domain affected Cx43CT residues Y265-L278 and G285-D339 (Fig. 7 *D*, *top*), whereas the affected Cx40CT residues span from F264-G285, E306-Q316, and Q332-S336 (Fig. 7 *E*, *top*). The K_D values are similar to those collected using ^{15}N-labled Cx45CT. These residues are similar to those previously described for the interactions between Cx40CT and Cx43CT (Fig. 7, *D* and *E*, *bottom*; 13, 16, 17, 27).

Characterization of the Cx45CT attached to the 4th transmembrane (TM4) domain

The soluble CT domain retains biochemical and functional properties consistent with those found in a gap junction plaque (16,17,25). However, when the Cx43CT was tethered to its 4th transmembrane domain (TM4-Cx43CT), the overall structure and structural responsiveness to stimuli (e.g., pH and phosphorylation) were different from the soluble form (53,54). Therefore, the TM4-Cx45CT and TM4 domain alone were purified and reconstituted in detergent micelles to characterize the effect of pH on its structure and to determine if dimerization occurs with this more native-like construct. The CD spectra for the soluble Cx45CT, TM4-Cx45CT, and TM4 domains are shown in Fig. 8. The TM4-Cx45CT had increased α-helical content (pH 5.8, 28%; pH 7.5, 25%; Fig. 2 *A*) in comparison to the soluble Cx45CT (pH 5.8, 19%; pH 7.5, 18%), whereas the TM4 domain alone was entirely α-helical. The TM4 domain contains ~9% of the total number of amino acids; combining this α-helical content with the soluble Cx45CT domain equates to that of the TM4-Cx45CT. Therefore, tethering the CT domain does not affect the α-helical content in the Cx45 isoform. Furthermore, the soluble Cx45CT and TM4 domains alone show minimal to no difference in secondary structure between the CD spectra collected at pH 7.5 and pH 5.8, whereas the TM4-Cx45CT had a small increase of α-helical content under acidification conditions. These data are different from the TM4-Cx43CT; the addition of the TM4 residues to the Cx43CT domain induced α-helical structure in the CT domain at physiological pH, which significantly increased upon acidification (53). Of note, LPPG had little-to-no effect on the Cx45CT secondary structure as determined by CD (Fig. S10; α-helical content in the presence (20%) or absence (19%) of LPPG).

Diffusion ordered spectroscopy NMR was used to determine if the TM4-Cx45CT was in a dimer conformation when solubilized in LPPG micelles. The diffusion rate of TM4-Cx45CT in LPPG (4.751 E-11 m^2/s) increased in the presence of 30% acetonitrile (9.002 E-11 m^2/s), indicating that acetonitrile disrupts Cx45CT dimerization. Dynamic light scattering confirmed this observation, as the hydrodynamic radius (R_H) representing protein was reduced from 144.6 nm to 31.5 nm in the presence of 30% acetonitrile (Fig. S11 and Table S4). Dynamic light scattering data also indicated that LPPG micelles remain intact in 30% acetonitrile only when protein is present in the solution. This observation, and that acetonitrile affects Cx45CT dimerization, is consistent with previously published ^{15}N-HSQC NMR data (28). In the ^{15}N-HSQC spectrum, 30% acetonitrile was needed to visualize all the crosspeaks. This is identical to what was observed with the soluble Cx45CT constructs (27), which are monomeric in 30% acetonitrile as determined by sedimentation equilibrium and velocity.

DISCUSSION

Biophysical characterization of the Cx45CT identified one region of α-helical structure flanked by two intrinsically disordered domains. The α-helical structure mediated dimerization through hydrophobic contacts. The

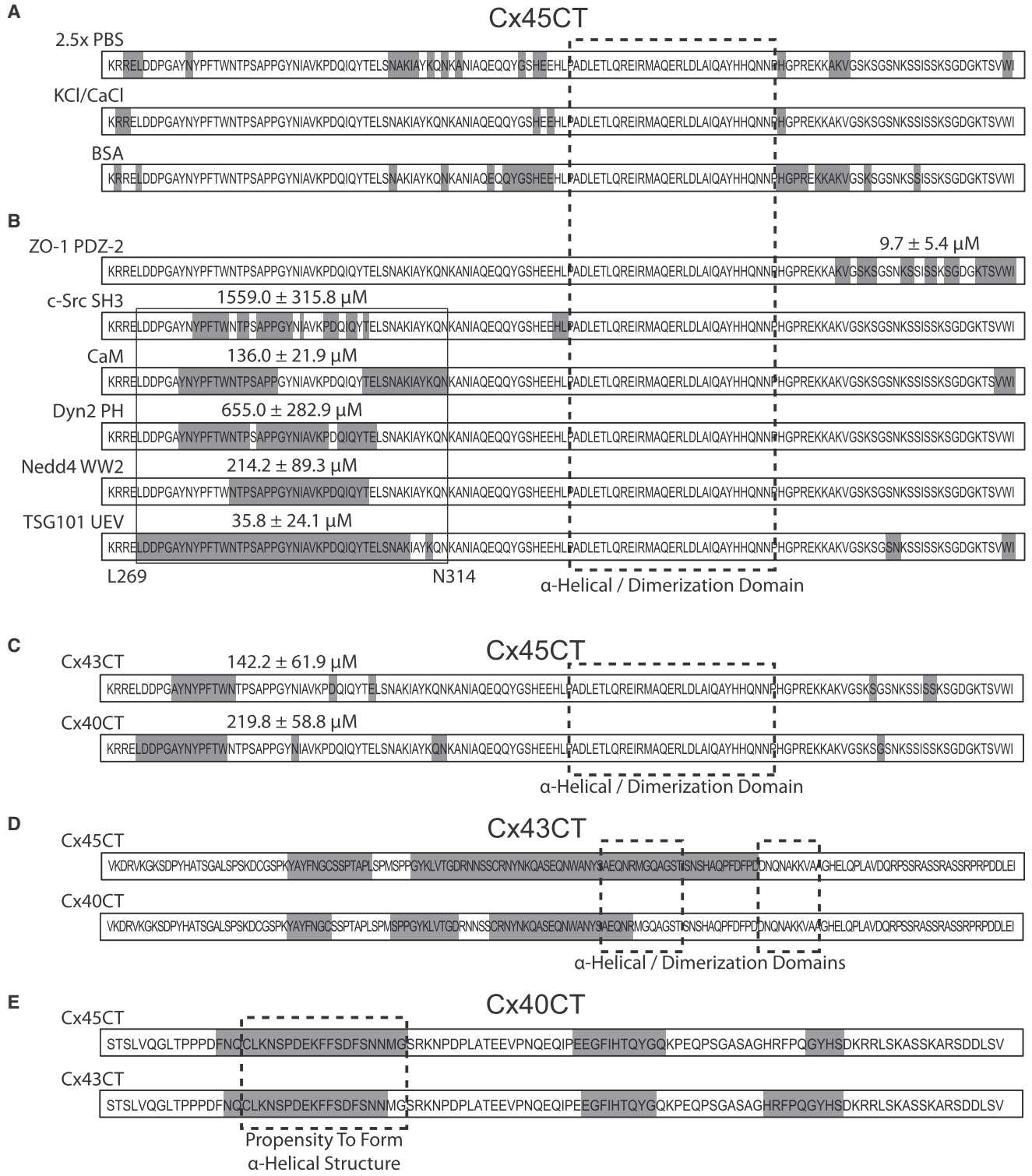

FIGURE 7 Summary of the Cx45CT residues affected by different molecular partners. For all panels, the affected CT residues from the ^{15}N-HSQC experiments are highlighted in gray and titrated partner is labeled on the left of each primary sequence. (*A*) Cx45CT residues susceptible to shifting by nonspecific effects (*controls*). (*B*) Cx45CT residues affected by each of the molecular partners. (*C–E*) Cx45CT, Cx43CT, and Cx40CT residues affected by each other. Data previously published for the Cx43CT/Cx40CT interaction are provided for comparison (13).

intrinsically disordered domains interacted with the same molecular partners as Cx43 and Cx40, as well as their CT domains. To our knowledge, this study represents the first structural characterization of the Cx45CT domain alone or when associated with molecular partners involved in gap junction regulation. These findings provide insight into the

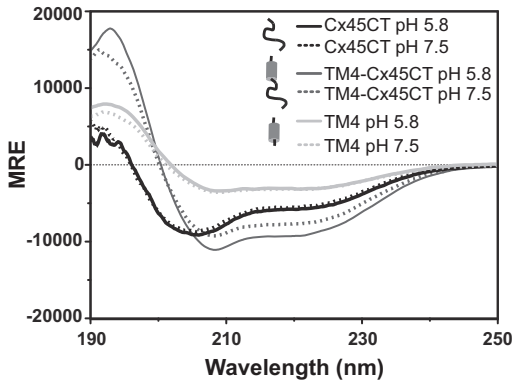

FIGURE 8 Secondary structure of the Cx45CT domain when attached to its 4th transmembrane domain. CD spectra are overlaid for the soluble Cx45CT K265-I396 (*black*), TM4-Cx45CT D219-I396 (*dark gray*), and TM4 domain D219-K314 (*light gray*) at pH 5.8 (*solid*) and pH 7.5 (*dashed*).

molecular mechanisms involved in the regulation of homomeric and heteromeric gap junctional channels.

Significance of the CT α-helical structure

In general, the structure of the Cx45, Cx43, and Cx40 CT domains are predominantly intrinsically disordered with varying degrees of α-helical content. The Cx40CT domain is entirely random coiled, albeit one region (C267-G285) has a propensity to form a α-helix in the presence of TFE (13). The Cx43CT structure is mostly intrinsically disordered with two short dynamic helical domains (5% total α-helical content) between A315-T326 and D340-A348 (14). The Cx45CT domain contains the largest amount of α-helical structure (19% total α-helical content), which is within one region (A333-N361). Almost no sequence homology exists between the α-helical residues of the Cx45CT and Cx43CT domains, yet their α-helical residues would be similarly located (distance from the membrane).

Residues within the Cx45CT and Cx43CT α-helices mediate CT homodimerization (27,29). The amount of α-helical content correlates with the binding affinity for the homodimer; the Cx45CT binding affinity is ~1000-fold stronger than that for the Cx43CT domain (pH 5.8, K_D = 141 nM vs. 70 μM, respectively; (13,29)). Our data indicate that Cx45CT dimerization is mediated by hydrophobic residues, potentially through a coiled-coil structure, as evident by the effects of solution conditions and mutations that specifically disrupt hydrophobic contacts. In contrast, no discernible hydrophobic face is evident in a helical wheel of the two small Cx43CT α-helical domains that mediate dimerization. We also identified that dimerization mediated by Cx45CT hydrophobic face is not pH-sensitive (97 nM at pH 7.5 and 141 nM at pH 5.8), but the nonhydrophobic dimerization of Cx43 is pH-sensitive (29,16). Furthermore, pH-mediated channel closure of Cx43 involves the CT domain but is not required for pH-mediated closure of Cx45 channels (13,25,56). Altogether, the data suggest that CT dimerization plays regulatory roles in connexin channels, and isoform-specific mechanisms and effects exist between the different cardiac connexins.

Cx43 and Cx45 can interact to form heteromeric gap junction channels in heterologous expression systems and in working ventricular myocytes (4,57–59). The physiological consequences of heteromeric gap junction channel formation on intercellular communication remain unclear; however, functional studies of heteromeric connexons show gating and permeability properties that differ from their homomeric counterparts (60). For example, expression of Cx45 in cells expressing Cx43 results in a dominant negative effect of Cx45 characterized by reduced gap junction conductance and dye transfer (4,59,61,62) without changes in Cx43 abundance, localization, or phosphorylation (62). Although the transmembrane domains have been implicated in the formation and regulation of gap junction channels (63,21), previous studies and those presented herein would also suggest involvement of the CT domain in regulation of heteromeric channels (25,62,65). Our data identified heterodimerization between the Cx45 and Cx43 CT domains; the residues involved in heterodimerization differ than those of homodimerization (Fig. 7, *C* and *D*; (13,29)). Because Cx45 dominates the conduction and dye-transfer phenotypes of Cx43/Cx45 heteromeric channels (4), the possibility exists that Cx45CT molecules forming dimers within the hexameric channels are sufficient to predominantly mimic a Cx45 channel rather than a Cx43 channel. Because the binding affinity of a Cx45CT/Cx43CT dimer is far stronger than that of a Cx43CT homodimer, heterodimerization (i.e., involving Cx43 and Cx45 CT domains) may occur at physiological pH, at which Cx43CT-Cx43CT dimerization would not occur. In either case, it would be important to inhibit Cx45CT homo- and heterodimerization in heteromeric channels, as our hypothesis would suggest that channel properties would then more resemble that of Cx43 homomeric channels.

Significance of the CT intrinsically disordered domains

The other important structural feature of the Cx43, Cx40, and Cx45 CT domains is that they are all predominantly intrinsically disordered. The major functions of intrinsically disordered proteins include protein-protein binding, flexibility, and phosphorylation, which all apply to the CT domains (66). A disordered CT domain would be ideal for cell signaling events by allowing many different binding partners with both high specificity and low affinity to rapidly switch between molecular partners, thus activating alternative signaling pathways (66). Numerous studies have identified molecular partners that interact with the CT domain of connexins (for review, see (8)). Identical to what was previously seen with the Cx43CT and Cx40CT domains, all of the

molecular partners studied here interacted in the intrinsically disordered regions of the Cx45CT (Table S5). For example, the PDZ-2 domain of ZO-1 affected most of the 26 C-terminal residues (K371-I396; $K_D = 9.7\ \mu M$), a region similar to that found in Cx40CT (last 28 residues; $K_D = 27.6\ \mu M$) and Cx43CT (last 19 residues; $K_D = 63\ \mu M$) (14,15). One Cx45CT region (residues Y275-Y290) was affected by most of the investigated molecular partners. These include the c-Src SH3, Nedd4 WW2, Dyn2 PH, and TSG101 UEV domains, which have overlapping sequence interacting motifs (SH3, PXXP; WW, PPXY; PH, polyproline; UEV, P[S/T]AP) within residues P282-Y288 (PSAPPGY). For CaM, a classical binding motif does not exist in the Cx45CT, suggesting a nontraditional binding motif similar to what was observed for Cx32CT (67,68). In general, the location and cellular conditions, along with post-translational modifications, will dictate which protein associates with the CT domain. We also identified that residues within this Cx45CT domain (P278-P285) undergo *cis-trans* proline isomerization (27). Previous reports identified that *cis-trans* proline isomerization can modulate protein-protein interactions (69). Although *cis-trans* proline isomerization has not been identified experimentally to occur for any other connexin CT domain, upon comparing the primary sequences, similarities exist between the CT domains of all identified cardiac connexins: Cx45 Y275-Y290, Cx43 S272-Y286, Cx40 P251-F265, Cx37 P266-Y279, and Cx30.2 P228-Y245 (Fig. 9). The online program CISPEPpred (sunflower.kuicr.kyoto-u.ac.jp/~sjn/cispep) predicted that all of these CT regions, except Cx43, can undergo *cis-trans* proline isomerization. Finally, this region within Cx43CT (S272-Y286) contains known sites of phosphorylation by MAPK, which decreases gap junction intercellular communication and modulates protein-protein interactions (i.e., Nedd4). Using the NetPhosK 1.0 server (www.cbs.dtu.dk/services/NetPhosK), the other cardiac connexins were predicted to also be phosphorylated within these regions (70). We propose that these CT residues constitute a master regulatory domain, an intrinsically disordered region that has known (or predicted) sites of phosphorylation, ability to undergo *cis-trans* proline isomerization, and overlapping sequence motifs that enables binding with multiple molecular partners (14,15).

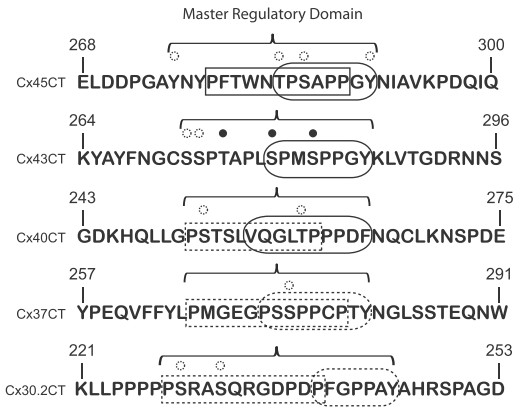

FIGURE 9 Schematic of the cardiac connexins' master regulatory domain. The proposed Cx45CT, Cx43CT, Cx40CT, Cx37CT, and Cx30.2 master regulatory domains are denoted by the brackets. The overlapping molecular partner sequence motifs are highlighted by the ovals. Sites of phosphorylation (*circles above sequences*) and *cis-trans* proline isomerization (*rectangles*) are indicated. Experimental data, solid lines; predicted data, dashed lines.

The CT domain of connexins contains many functionally important sites, notably those involved in channel gating, phosphorylation, and protein-protein interactions. As a key player in the regulation of gap junctions, the CT presents itself as a target for manipulation intended to modify function. Cx45 is predominately expressed in the specialized myocytes of the impulse generation and conduction system. In both ventricular and atrial human working myocardium, Cx45 is present in very low quantities; however, a reduction in ventricular Cx43 coupled with increased Cx45 protein levels has been observed after myocardial infarction and end-stage heart failure. Cx45 may influence electrical and/or metabolic coupling as a result of pathophysiological over-expression. A target would be to modify the behavior of the Cx45 channel to restore function (e.g., attenuate Cx45 dimerization to resemble Cx43 channels); this may prove valuable in the clinical management of arrhythmias in heart failure. The information provided from this and other studies will help build the foundation for the design of the next generation of chemical modifiers to achieve this goal.

SUPPORTING MATERIAL

Eleven figures, five tables, supporting data, and references (71–79) are available at http://www.biophysj.org/biophysj/supplemental/S0006-3495(14)00381-6.

The authors thank Ed Ezell for his assistance with NMR. We also thank the UNMC Structural Biology Facility for technical help and useful discussion regarding dynamic light scattering.

This work was funded by the United States Public Health Service Grant (GM072631). J.L.K. was funded by the Graduate Assistance in Areas of National Need Fellowship (P200A070554 and P200A090064). The UNMC Structural Biology Facility is funded by National Cancer Institute Eppley Cancer Center Support Grant (P30CA036727), National Center for Research Resources Grant (5P0RR016469), and the National Institute for General Medical Science Grant (8P20GM103427).

REFERENCES

1. Söhl, G., and K. Willecke. 2003. An update on connexin genes and their nomenclature in mouse and man. *Cell Commun. Adhes.* 10:173–180.

2. Severs, N. J., A. F. Bruce, …, S. Rothery. 2008. Remodelling of gap junctions and connexin expression in diseased myocardium. *Cardiovasc. Res.* 80:9–19.

3. Betsuyaku, T., N. S. Nnebe, …, K. A. Yamada. 2006. Overexpression of cardiac connexin45 increases susceptibility to ventricular

tachyarrhythmias in vivo. *Am. J. Physiol. Heart Circ. Physiol.* 290:H163–H171.

4. Martinez, A. D., V. Hayrapetyan, …, E. C. Beyer. 2002. Connexin43 and connexin45 form heteromeric gap junction channels in which individual components determine permeability and regulation. *Circ. Res.* 90:1100–1107.
5. Yamada, K. A., J. G. Rogers, …, J. E. Saffitz. 2003. Up-regulation of connexin45 in heart failure. *J. Cardiovasc. Electrophysiol.* 14:1205–1212.
6. Laird, D. W. 2010. The gap junction proteome and its relationship to disease. *Trends Cell Biol.* 20:92–101.
7. Lampe, P. D., and A. F. Lau. 2004. The effects of connexin phosphorylation on gap junctional communication. *Int. J. Biochem. Cell Biol.* 36:1171–1186.
8. Hervé, J.-C., N. Bourmeyster, …, H. S. Duffy. 2007. Gap junctional complexes: from partners to functions. *Prog. Biophys. Mol. Biol.* 94:29–65.
9. Unger, V. M., N. M. Kumar, …, M. Yeager. 1999. Three-dimensional structure of a recombinant gap junction membrane channel. *Science.* 283:1176–1180.
10. Maeda, S., S. Nakagawa, …, T. Tsukihara. 2009. Structure of the connexin 26 gap junction channel at 3.5 A resolution. *Nature.* 458:597–602.
11. Sorgen, P. L., H. S. Duffy, …, M. E. Girvin. 2002. Sequence-specific resonance assignment of the carboxyl terminal domain of Connexin43. *J. Biomol. NMR.* 23:245–246.
12. Bouvier, D., F. Kieken, and P. L. Sorgen. 2007. (1)H, (13)C, and (15)N backbone resonance assignments of the carboxyl terminal domain of Connexin40. *Biomol. NMR Assign.* 1:155–157.
13. Bouvier, D., G. Spagnol, …, P. L. Sorgen. 2009. Characterization of the structure and intermolecular interactions between the connexin40 and connexin43 carboxyl-terminal and cytoplasmic loop domains. *J. Biol. Chem.* 284:34257–34271.
14. Sorgen, P. L., H. S. Duffy, …, D. C. Spray. 2004. Structural changes in the carboxyl terminus of the gap junction protein connexin43 indicates signaling between binding domains for c-Src and zonula occludens-1. *J. Biol. Chem.* 279:54695–54701.
15. Bouvier, D., F. Kieken, …, P. L. Sorgen. 2008. Structural changes in the carboxyl terminus of the gap junction protein connexin 40 caused by the interaction with c-Src and zonula occludens-1. *Cell Commun. Adhes.* 15:107–118.
16. Hirst-Jensen, B. J., P. Sahoo, …, P. L. Sorgen. 2007. Characterization of the pH-dependent interaction between the gap junction protein connexin43 carboxyl terminus and cytoplasmic loop domains. *J. Biol. Chem.* 282:5801–5813.
17. Duffy, H. S., P. L. Sorgen, …, D. C. Spray. 2002. pH-dependent intramolecular binding and structure involving Cx43 cytoplasmic domains. *J. Biol. Chem.* 277:36706–36714.
18. Li, X., V. Su, …, A. F. Lau. 2008. A novel connexin43-interacting protein, CIP75, which belongs to the UbL-UBA protein family, regulates the turnover of connexin43. *J. Biol. Chem.* 283:5748–5759.
19. Moreno, A. P., and A. F. Lau. 2007. Gap junction channel gating modulated through protein phosphorylation. *Prog. Biophys. Mol. Biol.* 94:107–119.
20. Sosinsky, G. E., J. L. Solan, …, P. D. Lampe. 2007. The C-terminus of connexin43 adopts different conformations in the Golgi and gap junction as detected with structure-specific antibodies. *Biochem. J.* 408:375–385.
21. Beahm, D. L., A. Oshima, …, G. E. Sosinsky. 2006. Mutation of a conserved threonine in the third transmembrane helix of alpha- and beta-connexins creates a dominant-negative closed gap junction channel. *J. Biol. Chem.* 281:7994–8009.
22. Lal, R., S. A. John, …, M. F. Arnsdorf. 1995. Heart gap junction preparations reveal hemiplaques by atomic force microscopy. *Am. J. Physiol.* 268:C968–C977.
23. Allen, M. J., J. Gemel, …, R. Lal. 2011. Atomic force microscopy of Connexin40 gap junction hemichannels reveals calcium-dependent three-dimensional molecular topography and open-closed conformations of both the extracellular and cytoplasmic faces. *J. Biol. Chem.* 286:22139–22146.
24. Fort, A. G., and D. C. Spray. 2009. Trifluoroethanol reveals helical propensity at analogous positions in cytoplasmic domains of three connexins. *Biopolymers.* 92:173–182.
25. Stergiopoulos, K., J. L. Alvarado, …, M. Delmar. 1999. Hetero-domain interactions as a mechanism for the regulation of connexin channels. *Circ. Res.* 84:1144–1155.
26. D'hondt, C., J. Iyyathurai, …, G. Bultynck. 2013. Negatively charged residues (Asp-378 and Asp-379) in the last ten amino acids of the C-terminal tail of Cx43 hemichannels are essential for loop/tail interactions. *Biochem. Biophys. Res. Commun.* 432:707–712.
27. Kopanic, J. L., and P. L. Sorgen. 2013. Chemical shift assignments of the connexin45 carboxyl terminal domain: monomer and dimer conformations. *Biomol. NMR Assign.* 7:293–297.
28. Kopanic, J. L., M. Al-Mugotir, …, P. L. Sorgen. 2013. An *Escherichia coli* strain for expression of the connexin45 carboxyl terminus attached to the 4th transmembrane domain. *Front. Pharmacol.* 4:106.
29. Sorgen, P. L., H. S. Duffy, …, M. Delmar. 2004. pH-dependent dimerization of the carboxyl terminal domain of Cx43. *Biophys. J.* 87:574–581.
30. Duffy, H. S., A. W. Ashton, …, D. C. Spray. 2004. Regulation of connexin43 protein complexes by intracellular acidification. *Circ. Res.* 94:215–222.
31. Gopalakrishna, R., and W. B. Anderson. 1982. Ca2+-induced hydrophobic site on calmodulin: application for purification of calmodulin by phenyl-Sepharose affinity chromatography. *Biochem. Biophys. Res. Commun.* 104:830–836.
32. Hayashi, N., M. Matsubara, …, H. Taniguchi. 1998. An expression system of rat calmodulin using T7 phage promoter in Escherichia coli. *Protein Expr. Purif.* 12:25–28.
33. Provencher, S. W., and J. Glöckner. 1981. Estimation of globular protein secondary structure from circular dichroism. *Biochemistry.* 20:33–37.
34. Lees, J. G., A. J. Miles, …, B. A. Wallace. 2006. A reference database for circular dichroism spectroscopy covering fold and secondary structure space. *Bioinformatics.* 22:1955–1962.
35. Whitmore, L., and B. A. Wallace. 2004. DICHROWEB, an online server for protein secondary structure analyses from circular dichroism spectroscopic data. *Nucleic Acids Res.* 32 (Web Server issue):W668–W673.
36. Whitmore, L., and B. A. Wallace. 2008. Protein secondary structure analyses from circular dichroism spectroscopy: methods and reference databases. *Biopolymers.* 89:392–400.
37. Johnson, B. A. 2004. Using NMRView to visualize and analyze the NMR spectra of macromolecules. *Methods Mol. Biol.* 278:313–352.
38. Delaglio, F., S. Grzesiek, …, A. Bax. 1995. NMRPipe: a multidimensional spectral processing system based on UNIX pipes. *J. Biomol. NMR.* 6:277–293.
39. Kay, L., P. Keifer, and T. Saarinen. 1992. Pure absorption gradient enhanced heteronuclear single quantum correlation spectroscopy with improved sensitivity. *J. Am. Chem. Soc.* 114:10663–10665.
40. Farnum, M., and C. Zukoski. 1999. Effect of glycerol on the interactions and solubility of bovine pancreatic trypsin inhibitor. *Biophys. J.* 76:2716–2726.
41. Zangi, R., R. Zhou, and B. J. Berne. 2009. Urea's action on hydrophobic interactions. *J. Am. Chem. Soc.* 131:1535–1541.
42. Gekko, K., E. Ohmae, …, T. Takagi. 1998. Acetonitrile-protein interactions: amino acid solubility and preferential solvation. *Biochim. Biophys. Acta.* 1387:195–205.
43. Downing, A. K., and P. Guntert. 2004. Protein NMR Techniques. Humana Press, New Jersey.

44. Chen, R., L. Li, and Z. Weng. 2003. ZDOCK: an initial-stage protein-docking algorithm. *Proteins.* 52:80–87.

45. Laing, J. G., M. Koval, and T. H. Steinberg. 2005. Association with ZO-1 correlates with plasma membrane partitioning in truncated connexin45 mutants. *J. Membr. Biol.* 207:45–53.

46. Laing, J. G., R. N. Manley-Markowski, …, T. H. Steinberg. 2001. Connexin45 interacts with zonula occludens-1 and connexin43 in osteoblastic cells. *J. Biol. Chem.* 276:23051–23055.

47. Laing, J. G., R. N. Manley-Markowski, …, T. H. Steinberg. 2001. Connexin45 interacts with zonula occludens-1 in osteoblastic cells. *Cell Commun. Adhes.* 8:209–212.

48. Laing, J. G., J. E. Saffitz, …, K. A. Yamada. 2007. Diminished zonula occludens-1 expression in the failing human heart. *Cardiovasc. Pathol.* 16:159–164.

49. Kausalya, P. J., M. Reichert, and W. Hunziker. 2001. Connexin45 directly binds to ZO-1 and localizes to the tight junction region in epithelial MDCK cells. *FEBS Lett.* 505:92–96.

50. Valiunas, V., R. Weingart, and P. R. Brink. 2000. Formation of heterotypic gap junction channels by connexins 40 and 43. *Circ. Res.* 86:E42–E49.

51. Rackauskas, M., M. M. Kreuzberg, …, F. F. Bukauskas. 2007. Gating properties of heterotypic gap junction channels formed of connexins 40, 43, and 45. *Biophys. J.* 92:1952–1965.

52. Rackauskas, M., V. K. Verselis, and F. F. Bukauskas. 2007. Permeability of homotypic and heterotypic gap junction channels formed of cardiac connexins mCx30.2, Cx40, Cx43, and Cx45. *Am. J. Physiol. Heart Circ. Physiol.* 293:H1729–H1736.

53. Kellezi, A., R. Grosely, …, P. L. Sorgen. 2008. Purification and reconstitution of the connexin43 carboxyl terminus attached to the 4th transmembrane domain in detergent micelles. *Protein Expr. Purif.* 59:215–222.

54. Grosely, R., J. L. Kopanic, …, P. L. Sorgen. 2013. Effects of phosphorylation on the structure and backbone dynamics of the intrinsically disordered connexin43 C-terminal domain. *J. Biol. Chem.* 288:24857–24870.

55. Reference deleted in proof.

56. Palacios-Prado, N., S. W. Briggs, …, F. F. Bukauskas. 2010. pH-dependent modulation of voltage gating in connexin45 homotypic and connexin45/connexin43 heterotypic gap junctions. *Proc. Natl. Acad. Sci. USA.* 107:9897–9902.

57. Bao, M., E. M. Kanter, …, S. Maxeiner. 2011. Channels: Research Paper.

58. Elenes, S., A. D. Martinez, …, A. P. Moreno. 2001. Heterotypic docking of Cx43 and Cx45 connexons blocks fast voltage gating of Cx43. *Biophys. J.* 81:1406–1418.

59. Bukauskas, F. F., A. B. Angele, …, M. V. L. Bennett. 2002. Coupling asymmetry of heterotypic connexin 45/ connexin 43-EGFP gap junctions: properties of fast and slow gating mechanisms. *Proc. Natl. Acad. Sci. USA.* 99:7113–7118.

60. Moreno, A. P. 2004. Biophysical properties of homomeric and heteromultimeric channels formed by cardiac connexins. *Cardiovasc. Res.* 62:276–286.

61. Moreno, A. P., J. G. Laing, …, D. C. Spray. 1995. Properties of gap junction channels formed of connexin 45 endogenously expressed in human hepatoma (SKHep1) cells. *Am. J. Physiol.* 268:C356–C365.

62. Koval, M., S. T. Geist, …, T. H. Steinberg. 1995. Transfected connexin45 alters gap junction permeability in cells expressing endogenous connexin43. *J. Cell Biol.* 130:987–995.

63. Smith, T. D., A. Mohankumar, …, M. Koval. 2012. Cytoplasmic amino acids within the membrane interface region influence connexin oligomerization. *J. Membr. Biol.* 245:221–230.

64. Reference deleted in proof.

65. Gu, H., J. F. Ek-Vitorin, …, M. Delmar. 2000. Coexpression of connexins 40 and 43 enhances the pH sensitivity of gap junctions: a model for synergistic interactions among connexins. *Circ. Res.* 86:E98–E103.

66. Dunker, A. K., C. J. Brown, …, Z. Obradović. 2002. Intrinsic disorder and protein function. *Biochemistry.* 41:6573–6582.

67. Stauch, K. L., F. Kieken, and P. L. Sorgen. 2012. Characterization of the structure and intermolecular interactions between the connexin 32 carboxyl-terminal domain and the protein partners synapse-associated protein 97 and calmodulin. *J. Biol. Chem.* 287:27771–27788.

68. Rhoads, A. R., and F. Friedberg. 1997. Sequence motifs for calmodulin recognition. *FASEB J.* 11:331–340.

69. Sarkar, P., C. Reichman, …, C. G. Kalodimos. 2007. Proline *cis-trans* isomerization controls autoinhibition of a signaling protein. *Mol. Cell.* 25:413–426.

70. Blom, N., T. Sicheritz-Pontén, …, S. Brunak. 2004. Prediction of post-translational glycosylation and phosphorylation of proteins from the amino acid sequence. *Proteomics.* 4:1633–1649.

71. Kieken, F., N. Mutsaers, …, P. L. Sorgen. 2009. Structural and molecular mechanisms of gap junction remodeling in epicardial border zone myocytes following myocardial infarction. *Circ. Res.* 104:1103–1112.

72. Török, K., K. Stauffer, and W. H. Evans. 1997. Connexin 32 of gap junctions contains two cytoplasmic calmodulin-binding domains. *Biochem. J.* 326:479–483.

73. Zhou, Y., W. Yang, …, J. J. Yang. 2007. Identification of the calmodulin binding domain of connexin 43. *J. Biol. Chem.* 282:35005–35017.

74. Gumpert, A. M., J. S. Varco, …, M. M. Falk. 2008. Double-membrane gap junction internalization requires the clathrin-mediated endocytic machinery. *FEBS Lett.* 582:2887–2892.

75. Nickel, B., M. Boller, …, S. A. Murray. 2013. Visualizing the effect of dynamin inhibition on annular gap vesicle formation and fission. *J. Cell Sci.* 126:2607–2616.

76. Gilleron, J., D. Carette, …, G. Pointis. 2011. The large GTPase dynamin2: a new player in connexin 43 gap junction endocytosis, recycling and degradation. *Int. J. Biochem. Cell Biol.* 43:1208–1217.

77. Leykauf, K., M. Salek, …, A. Alonso. 2006. Ubiquitin protein ligase Nedd4 binds to connexin43 by a phosphorylation-modulated process. *J. Cell Sci.* 119:3634–3642.

78. Auth, T., S. Schlüter, …, K. Willecke. 2009. The TSG101 protein binds to connexins and is involved in connexin degradation. *Exp. Cell Res.* 315:1053–1062.

79. Leithe, E., A. Kjenseth, …, E. Rivedal. 2009. Ubiquitylation of the gap junction protein connexin-43 signals its trafficking from early endosomes to lysosomes in a process mediated by Hrs and Tsg101. *J. Cell Sci.* 122:3883–3893.